https://doi.org/10.46813/2025-157-176

SBM1 MODE OF THE RPW/SOLAR ORBITER INSTRUMENT AS A PATHFINDER OF SOLAR WIND IRREGULARITIES IN THE INTERPLANETARY SPACE

D.L. Chechotkin[1], O.V. Dudnik[2,1], O.V. Yakovlev[1]
[1]Institute of Radio Astronomy of the National Academy of Sciences of Ukraine, Kharkiv, Ukraine;
[2]Space Research Centre of the Polish Academy of Sciences, Warsaw, Poland
E-mail: chechotkin@rian.kharkov.ua

Discontinuities and irregularities in large-scale solar wind (SW) structures are one of the main sources of disturbances that are transferred from the Sun to the Earth's magnetosphere and cause various space weather phenomena. The paper analyzes the possibility of using SBM1 trigger events of the RPW instrument of the Solar Orbiter space mission as markers of the presence of compression regions and other irregularities in the SW streams. Using examples, it is shown that multiple SBM1 trigger events over an interval of up to four hours show the fine structure of large-scale variations in the SW parameters, and such trigger events can be used as a marker of the spacecraft location in the compression region.

PACS: 95.55.-n; 95.75.-z; 96.90.+c

INTRODUCTION

The structure of the Solar Wind (SW) in the heliosphere is highly inhomogeneous. Its speed, density, temperature, magnetic field magnitude and direction show great variations on different time scales. The SW structure is characterized by large-scale variations, including quasi-stationary High-Speed Streams (HSSs) emanating from Coronal Holes (CHs), slow streams outflowing mainly from near-equatorial regions and streamers, Heliospheric Current Sheets (HCSs), and transient SW streams associated with interplanetary coronal mass ejections (ICMEs) [1 with references].

The interaction of large-scale streams causes small-scale fluctuations in parameters and makes the so-called irregularities or discontinuities in SW streams [2]. Among them are shock waves, compression regions, tangential and rotational discontinuities. Compression regions and shock waves demonstrate the greatest geoefficiency in the system of solar-terrestrial relations [3, 4].

Compressed plasma regions in the SW stream are formed when a high-speed SW stream propagates into a slower SW stream ahead, developing Stream Interaction Regions (SIRs) [5-7]. A high-speed stream emanating from a coronal hole can be observed over several solar rotations around the axis. As the Sun rotates, SIRs recur (corotate) with the Sun, hence the name Corotating Interaction Regions (CIRs) [6, 8]. The SIR/CIR influence on space weather is very diverse. These regions can modulate and scatter galactic cosmic rays [9] and lead to the acceleration of energetic particles [6, 10]. The interaction of SIR with ICME may produce perturbations like shock waves and tangential and rotational discontinuities [5, 11, 12]. This increases the geoefficiency of SIR structures when they reach the Earth's orbit. Causing irregularities in the Earth's ionospheric plasma in sporadic E_s layers, SIRs can significantly affect radio communication and navigation systems [13].

Let us consider the trajectory of Solar Orbiter (SolO) flight 2023-2024 (Fig. 1) relative to the Earth and the Sun. As seen, SolO stays east of the Earth at angles 0 to 30^0 for more than five months of the year. This fact can be used to predict the time of SIR/CIR arrival to the Earth. The western (as viewed from the Earth) portion of the SolO trajectory is also suited for this purpose. In this case, however, allowance must be made for a delay of more than half of the Carrington period. Notice, that the CH structure cannot stay unchanged for so long.

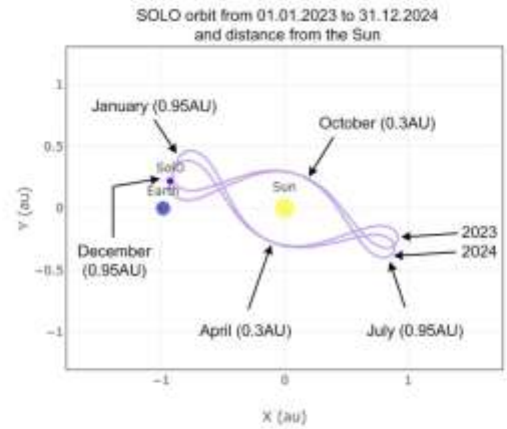

Fig. 1. The SolO flight trajectory relative to the Earth and the Sun in the ecliptic plane, 2023–2024

Our study uses the data from the SolO instruments Solar Wind Analyzer (SWA) [14], Magnetometer (MAG) [15], and Radio and Plasma Wave (RPW) [16]. Trigger mode data from the SolO instruments are promptly transmitted for the general scientific community's access within a few days and even sooner for special services. For comparison, SW and IMF (Interplanetary Magnetic Field) data on level L2 are available for the general scientific community no sooner than in three months [14-21]. Due to this logic of equipment operation and scientific data release, the use of trigger modes will accelerate the detection and identification of geoeffective SW structures, such as

SIR, interplanetary shock (IPS) waves, and heliospheric current sheets, thereby enhancing space weather forecasting.

1. METHODOLOGY

1.1. PECULIARITIES OF RPW OPERATION IN TRIGGER MODE

The RPW instrument has two trigger modes, SBM1 and SBM2 (Survey Burst Modes 1 and 2) [16]. SBM1 fits the shock wave registration in interplanetary space. SBM2 is suitable for registering type III radio bursts, associated density fluctuations, and Langmuir waves.

The SBM1 trigger mode is based on the algorithm for detecting IPS waves of various types [17]. The SBM1 algorithm detects combined temporal jumps in the interplanetary magnetic field strength, proton density, and SW stream speed.

The algorithm realizes the window-time averaging of the measured parameters over the interval Δt_{buff}. After that, the differences between adjacent time windows are calculated, yielding the decision criteria for triggering:

$$\frac{2|B_{t2} - B_{t1}|}{B_{t2} + B_{t1}} = \Delta B > \Delta B_{thr},$$

$$\frac{2|N_{t2} - N_{t1}|}{N_{t2} + N_{t1}} = \Delta N > \Delta N_{thr},$$

$$\frac{2|V_{t2} - V_{t1}|}{V_{t2} + V_{t1}} = \Delta V > \Delta V_{thr},$$

where

B_{t2} and B_{t1} are the average values of the interplanetary magnetic field intensity in adjacent time windows;

N_{t2} and N_{t1} are the average values of the SW proton density in adjacent time windows;

V_{t2} and V_{t1} are the SW speed average values in adjacent time windows, and $\Delta B_{thr}, N_{thr},$ and V_{thr} are the threshold values of the corresponding parameters.

The statistical testing from the algorithm developers for different input data and threshold values made it possible to conclude that the IPS detection using the described algorithm is a probabilistic event. Therefore, they introduced the quality factor (QF), a generalizing criterion of the SBM1 trigger mode algorithm performance. The QF is determined by the weighted sum of the averaged fluctuations of SW and IMF parameters over the analyzed time interval [17, 18]:

$$\alpha \Delta B + \beta \Delta N + \gamma \Delta V = QF > QF_{thr},$$

where $\alpha + \beta + \gamma = 1$ are the weight coefficients of the basic parameters and QF_{thr} is the quality factor threshold.

By varying the weight coefficients, time interval, and threshold value, the algorithm performance can be optimized for specific conditions, such as changeable heliocentric distance or temporal characteristics of irregularities in the stream.

Using the SBM1 RPW trigger event database in 2023-2024, we analyze the triggering in terms of the potential use of trigger events as markers of SolO presence within the SIR structure, HCS intersections, and other irregularities.

1.2. IDENTIFICATION METHODOLOGY FOR SIR AND OTHER IRREGULARITIES

Fig. 2 illustrates SBM1 triggering at different irregularities within the solar wind. In Fig. 2,i, SBM1 was triggered at the front of the fast forward shock (FFS) – at the ICME front (Sep 6, 2023, 20:23 UT). The signs of the ICME presence within the SW stream are its components – sheath and flux rope – well observed on the plots of the IMF components, Fig. 2,i(f). In Fig. 2,ii, SBM1 was triggered three times within 4.5 h at the HSS leading edge near the stream interface (Oct 24, 2023, the beginning of the day).

Although using the SBM1 trigger to identify FFS waves in SW and IMF parameters appears straightforward, applying the SBM1 trigger to detect SIR structures requires refining the trigger use methodology.

To identify SIR, it is necessary to recognize a compression region that includes an accelerated domain in a slow SW with an increased particle density and a decelerated but still increased-density domain at the HSS leading edge [19]. The confluence of different-velocity streams in the SW represents a tangential discontinuity called Stream Interface (SI). Since streams of varying velocities in the solar wind originate from various solar sources with distinct magnetic field parameters, the interpenetration of these streams is nearly nonexistent. A compression region can be recognized by a jump in the proton density, pressure, and IMF intensity, with an increase in temperature and plasma velocity, indicating the HSS presence [5, 20].

On the strength of the above, SIR is detected via SW plasma parameters, including proton density N_{SW}, pressure P_{SW}, velocity V_{SW}, and temperature T_{SW} provided by the SWA-PAS instrument. The SW plasma parameters are added by IMF parameters, such as module B_0 and projections B_r, B_t, and B_n onto the corresponding axes of the RTN coordinate system related to SolO [21, 22]. The SW and IMF plots have dotted lines indicating the triggering moments of SBM1 trigger events.

Based on these plots (see Fig. 2,ii), a search is made for HSS, and then compression regions are sought at the HSS leading edges. The SW speed (see Fig. 2,ii(c)) and temperature (see Fig. 2,ii(d)) show the HSS presence for more than four days. The compression region at the HSS leading edge is indicated by the jumps in proton density (see Fig. 2,ii(a)) and pressure (see Fig. 2,ii(b)).

As the SIR structure evolves, Forward and Reverse shocks are formed at the compression region boundaries and are often observed beyond 1 AU [10]. Ten-year studies [5] of SIR and CIR at a distance of 1 AU were performed using Wind and ACE spacecraft data to find out that only 24% of the recorded SIRs had Shocks. Of them, nearly 70% had Forward Shock, and about 24% had Reverse Shock.

The next step was to check whether Forward and Reverse shocks were present. Besides, SBM1 can trigger on these IPS. Thus, in the considered example (see Fig. 2,ii), the SIR was completed with a weak reverse IPS, but the jumps in the parameters did not exceed the SBM1 trigger thresholds. This might be because of a low growth of the SW speed parameter (see Fig. 2,ii(c)), and the SBM1 event was not detected by the instrument.

From the example considered, we can assume the selection criteria for SBM1 trigger events as markers of the SolO presence within the SIR. Specifically, these events are registered against the backdrop of the SW speed increase characteristic of the HSS. They do not exhibit any distinct signs of FFS waves and are recorded more than once within several hours.

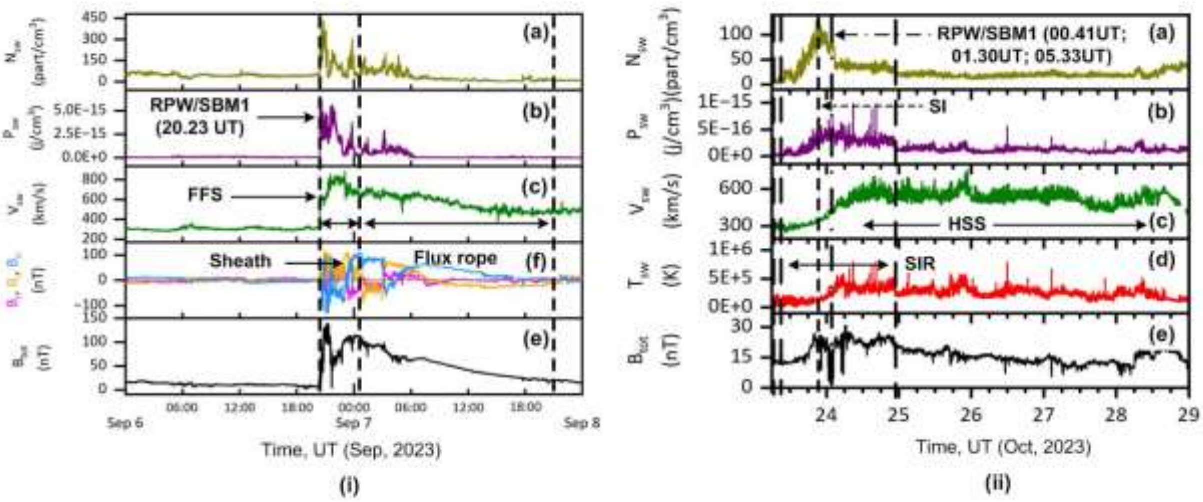

Fig. 2. Typical behavior of SW and IMF parameters during the observations with the SolO instruments: (i) FFS at the time of the SBM1 trigger event on 06.09.2023 and (ii) HSS with a compression region at the HSS leading edge on the interval 23.10.2023 to 29.10.2023. The panels display (a) proton density N_{SW}, (b) pressure P_{SW}, (c) velocity V_{SW}, (d) temperature T_{SW}, (e) IMF magnitude B_{tot}, and (f) IMF components B_r, B_t, and B_n

2. RESULTS AND DISCUSSION

2.1. STATISTICAL ANALYSIS OF SBM1 EVENTS IN 2023-2024

Taking into account the considered peculiarities of the SBM1 trigger mode operation and the probabilistic nature of the interplanetary shock registrations with the SBM1 algorithm, we systematized all SBM1-type events recorded in 2023-2024 to be listed in Table.

The thresholds of the SBM1 algorithm are optimized to detect such irregularities in the SW stream as Forward, Reverse, Fast, and Slow Shocks [18]. Fast Forward Shocks (FFSs) are often observed at the ICME front propagating at a speed exceeding 500 km/s. As a rule, these ICMEs are characterized by enhanced geoefficiency [2]. Considering the behavior of SW and IMF parameters at the SIR leading edge, we say that if a shock wave has formed on the SIR leading edge, it is an FFS wave [6, 8]. Therefore, the FFSs deserve an individual analysis and a particular column in Table. The FFS identification was performed with the proviso of intense growth of all the parameters (IMF intensity, SW speed, and proton density) involved in the SBM1 algorithm [17]. A condition was imposed on a parameter jump to be within a 6-min time window used in the SBM1 algorithm [18].

The considered period falls into the phase of solar cycle growth. During that period, SolO made four orbits around the Sun. The increased solar activity explains why the E_{SBM1} number of events registered in 2024 is higher than that in 2023.

The total number of E_{FFS}, which can correspond to SIR forward shocks, ICME events, or their interactions is about 8% for the two years. This number is somewhat lower than the result from the SBM1 algorithm developers [17]. In general, however, they do not contradict each other because, firstly, we did not count the number of slow and reverse shocks. Secondly, we do not have enough awareness of the other results from the algorithm testing in real situations.

The analysis of Fig. 2,i shows such a peculiarity that SBM1 was triggered three times in the SI region within four hours. The number of the days when SBM1 events repeat two or more times during a day (D_{repeat}) exceeds 55% of the total number of the days marked by at least one event recorded (D_{SBM1}). Notice that many solar phenomena, such as ICME or SIR, have temporal dynamic for a day or more. And, as the SBM1 events repeating during a single day may belong to the same solar phenomenon, they can provide additional information for their analysis.

Among repeating SBM1 events, quite a large group of events recurring within four hours (D_{repeat}^{4hh}) should be separated. The number of the days marked by such events amounts to more than 69% of the D_{repeat} days. We assume that such trigger events reflect the fine internal structure of the phenomenon during which the event is recorded and can correspond, e.g., for SIR/CIR, to their components. Also, it was observed that roughly within 10 to 12 h between successive SBM1 events, particular components of extended combined events can be detected, such as the overlaps ICME+ICME or ICME+SIR. Then, the first SBM1 event can correspond to FFS at the ICME front. The second represents FFS at the SIR leading edge.

Summary of SBM1 triggers in 2023-24

Year	E_{SBM1}	E_{FFS}	D_{SBM1}	D_{repeat}	D_{repeat}^{4hh}
Jan, 2023	18	1	13	4	4
2023	351	23	133	68	43
% from(i)	–	6.55% (E_{SBM1})	–	51.1% (D_{SBM1})	63.2% (D_{repeat})
2024	385	35	145	86	64
% from(i)	–	9.09% (E_{SBM1})	–	59.3% (D_{SBM1})	74.4% (D_{repeat})
$\sum$	736	58	278	154	107
% from(i)	–	7.88% (E_{SBM1})	–	55.4% (D_{SBM1})	69.4% (D_{repeat})

Here: E_{SBM1} is the total number of SBM1 trigger events during the given period, E_{FFS} is the number of SBM1 trigger events corresponding to FFS, D_{SBM1} is the number of the days marked by at least one SBM1 trigger, D_{repeat} is the number of the days when the trigger was registered no less than twice, and D_{repeat}^{4hh} is the number of the days when the trigger was repeatedly registered on an interval of up to 4 h. The statistics of SBM1 trigger events in January 2023 are highlighted on a separate line to be discussed in more detail in Section 2.2.

2.2. ANALYSIS OF SBM1 EVENTS IN JANUARY 2023

Let us take the SBM1 trigger events in January 2023 and consider them in more detail. During the mentioned period, the angular position of SolO as a component of the system SOLO-Sun-Earth varies from 22 to 30^0 to the east of the Earth-Sun direction. Therefore, the interplanetary events observed from SolO can be further identified using the data from the instruments onboard near-Earth satellites.

The vertical dashed lines in Fig. 3 mark SBM1 trigger events. The total number of the SBM1 events is given by the parameter E_{SBM1} in Table. The E_{FFS} event corresponding to the FFS registration in an SW stream is specially highlighted. The days with the repeating D_{repeat}^{4hh} events are also pointed out with the numbers of the SBM1 algorithm triggers. Though we lack measurements on some days (see data gaps in the plots in Fig. 3), it can be seen that SBM1 trigger events are observed against the background of four HSS events 3 to 5 days long each.

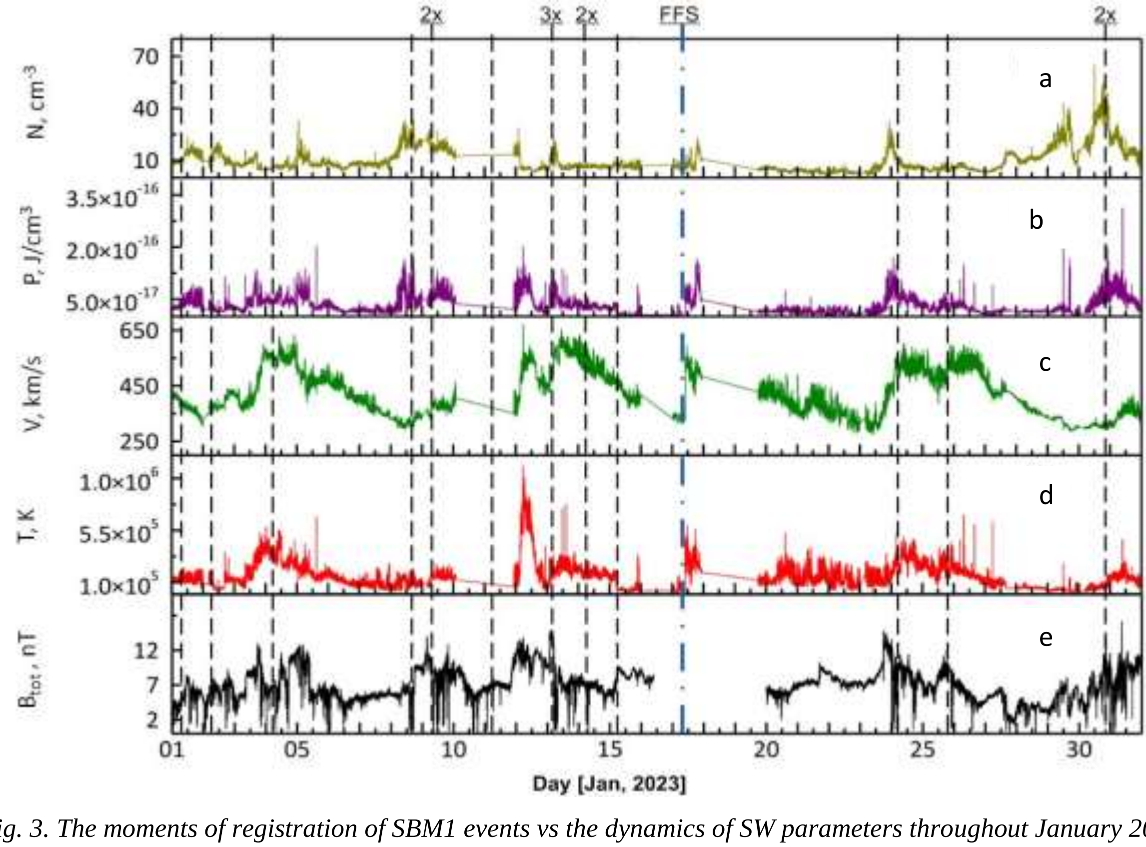

Fig. 3. The moments of registration of SBM1 events vs the dynamics of SW parameters throughout January 2023: (a) proton density N_p, (b) pressure P, (c) speed V_{SW}, (d) temperature T_{SW}, and (e) IMF magnitude B_{tot}. The vertical dotted lines refer to the SBM1 events corresponding to E_{SBM1} in Table. The FFS dash-dotted line marks the day of the E_{FFS} event registration, 2x and 3x are the numbers of repeated SBM1 events during the day

One E_{FFS} event was registered on Jan 17, 2023, at 09:56 UT. Its source is IPS at the ICME front. This ICME can be associated with the relevant record in the DONKI database (https://kauai.ccmc.gsfc.nasa.gov/DONKI) made on Jan 15, 2023, at 03:48 UT. This Coronal Mass Ejection (CME) was observed on the visible side of the solar disk in the southeast and confirmed with LASCO-C2 images. After this E_{FFS} event, HSS continues to be seen (see Fig. 3,c).

Fig. 3 shows that certain SBM1 trigger events are clustered where the density, pressure, and IMF intensity peak, and the HSS speed increases or approaches a maximum. Refer to January 8, 9, 13, 17, 24, and 30. On these days, except Jan. 17, the SBM1 events had occurred before the SW stream velocity started growing. They could correspond to the compression regions. The days Jan. 9, 13, and 30 are remarkable for the repeated triggering of the SBM1 algorithm where the density and the pressure of the SW stream are at their maxima.

According to [5, 8], it is the gradient of pressure that controls the evolution of SW structures. Also, the pressure signatures are simpler than the signatures of other SW components and, therefore, can be more informative. Since the pressure parameter is not used in the SBM1 algorithm [17], we persistently monitored the behavior of pressure against the background of other SW parameters and, therefore, present this parameter in our plots.

From what is considered in Fig. 3, we conclude that the SBM1 trigger events are repetitive over a four-hour interval, arise within large-scale SW structures and reflect their fine structure. Taking into account the fact that they occur at the local peaks of SW pressure and density at the HSS leading edge, they can serve as an additional indicator of the compression region's presence.

2.3. AN EXAMPLE OF SBM1 EVENTS OCCURRING AT DIFFERENT SW AND IMF DISCONTINUITIES (JANUARY 13-14, 2023)

Take up the above-discussed SBM1 threefold triggering of Jan. 13, 2023 and consider it in more detail. Fig. 4 displays the behavior of SW and IMF parameters on Jan. 13-14, 2023. At that time, the SolO distance to the Sun was $L_{SolO-Sun} = 0.95\ AU$, and the angle in the ecliptic plane was $\phi_{SolO-S-E} = 26°$ east of the central meridian. At the beginning of Jan. 13, RPW registered three events of SBM1 type.

Fig. 4,c indicates that the HSS stayed observable for about two days. At the HSS leading edge, we can see the interaction of two events. The SIR superimposes on the ICME moving ahead. A sharp jump in the SW and IMF parameters at 01:40 UT manifests the ICME presence of the FFS type. After the FFS, a flux rope within IMF components is seen (see Fig. 4,e).

The ICME presence at the leading edge makes for the deformation of the compression region. The accelerated area of the slow SW with HCS inside it is trapped between the ICME flux rope and the oncoming pressing HSS. The squeeze brings about intensive fluctuations of SW and IMF parameters and triggers the SBM1 trigger mode algorithm. According to Fig. 4,a,b, the trigger occurs at the pressure and SW proton density local peaks and near the centers of the compression regions.

We suggest that the source of this ICME might be the CME that was observed by SOHO/LASCO on Jan. 11, 2023, at about 09:00 UT on the northeastern limb of the solar disk with the record in the DONKI database (https://kauai.ccmc.gsfc.nasa.gov/DONKI).

The interaction between ICME and SIR occurred a little before the FFS registration by SWA-PAS. Presumably, it was at about 00:15 UT on Jan. 13, 2023. This is confirmed by the presence of the type III interplanetary radio burst on the radio spectrograms derived from the RPW/SolO, SWAVES/STEREO [23], and WAVES/WIND [24] instruments (Fig. 5). The interplanetary origin of this type III radio burst is indicated by the absence of a visible increase in the intensity at frequencies higher than 1 MHz. Moreover, we see the low frequency drift rate and the fact that the type III radio burst was registered by space instruments far situated from each other in the heliosphere. The increased intensity fluctuations in the plasma frequencies region (the bright area in all three spectrograms in the range of 500…700 kHz) also draw attention. This fact may tell us about the ICME and SIR interaction accompanied by the acceleration of SW plasma particles, which may be the source of interplanetary radio bursts [6, 10, 11, 25].

After the third SBM1 event at 07:40 UT on Jan. 13, 2023, there is a steady decay in the SW proton pressure and density until the background values. The curve of the SW rate reaches a plateau with $V_{SW} \approx 550$ km/s, followed by a smooth decay by 20:00 UT on Jan 14, 2023. Throughout this time, the parameters of density, pressure, and temperature of the SW stream demonstrate such equivalent quantitative parameters that are characteristic of the HSS.

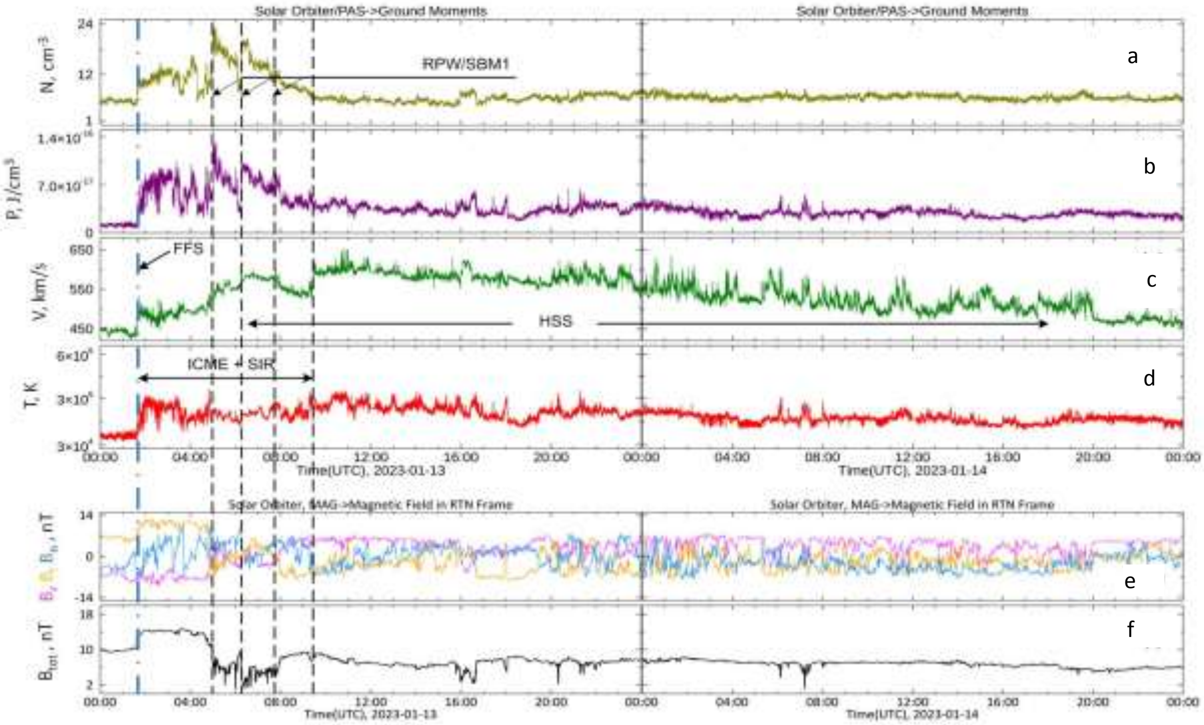

Fig. 4. The behavior of SW and IMF parameters on January 13–14, 2023: (a) proton density N_p, (b) pressure P, (c) velocity V_{SW}, (d) temperature T_{SW}, (e) IMF components B_r, B_t, B_n, and (f) IMF magnitude B_{tot}

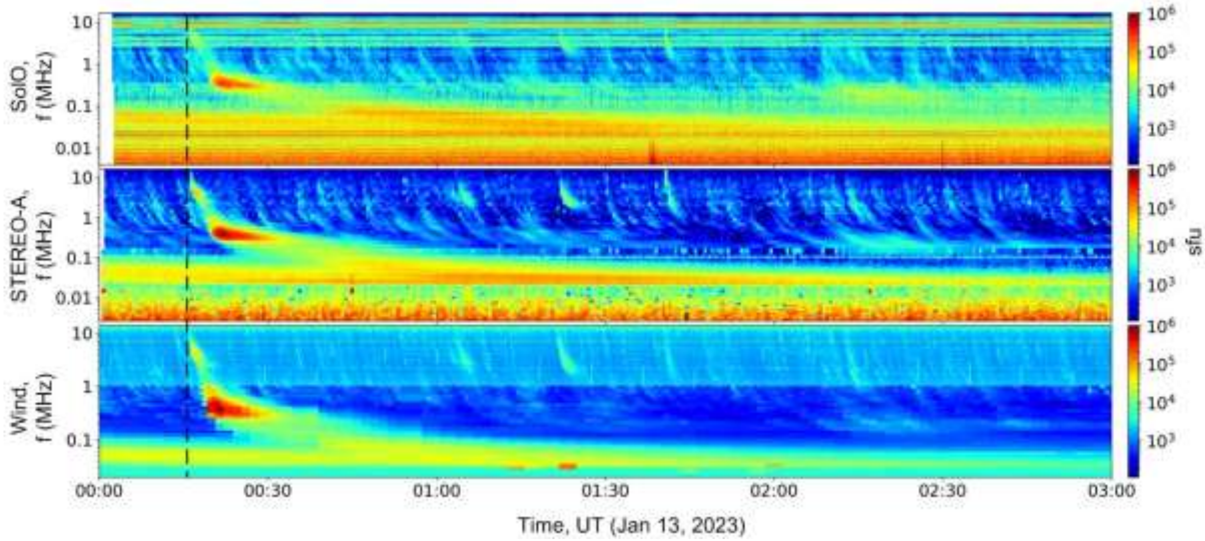

Fig. 5. Combined radio spectrograms from the RPW/SOLO, SWAVES/STEREO-A, and WAVES/WIND instruments. The vertical dotted line marks the beginning of the interplanetary type III radio burst corresponding to the region of the ICME and SIR interaction with the formation of accelerated particles, and sfu is a solar radio flux unit

CONCLUSIONS

The analysis of SBM1 triggers of the RPW/Solar Orbiter instrument registered in 2023-2024 has shown that they often occurred many times during a day. Taking into account the temporal dynamics of large-scale SW structures, we conclude that repeating SBM1 events reflect the internal variability of these structures.

Only 8% of the SBM1 triggers in 2023-2024 match FFS events observed at the ICME front and the SIR leading edge.

The fluctuations of SW and IMF parameters within the compression region can cause multiple triggering of the SBM1 trigger. These triggers occur at discontinuities and irregularities that can be reverse and forward shocks and heliospheric current sheet events.

The observational data show that successive SBM1 events bearing no distinct FFS signs and registered within two to four hours may indicate the SolO location inside SIR and HCS. Reliable conclusions about the SIR registration and characteristics can be drawn from the analysis of the SW and interplanetary magnetic field parameters from the SWA and MAG data.

Due to that the summary reports about SBM1 trigger events are transmitted in telemetric packages, the events of this type can be used in the operational analysis of the space weather to identify the compression regions and shocks at the ICME front.

ACKNOWLEDGEMENTS

This work is supported by the “Long-term program of support of the Ukrainian research teams at the Polish Academy of Sciences carried out in collaboration with the U.S. National Academy of Sciences with the financial support of external partners”, Agreement No. PAN.BFB.S.BWZ.363.022.2023.

The authors express their gratitude to the scientific and technical group of the RPW, SWA, and MAG teams of the Solar Orbiter Mission and the NOAA Space Weather Prediction Center for free access to the data.

REFERENCES

1. Y.I. Yermolaev, I. Lodkina, G. Khokhlachev, et al. Drop of solar wind at the end of the 20th century // *J. Geophys. Res. Space Physics*. 2021, v. 126, id. e2021JA029618. https://doi.org/10.1029/2021JA029618

2. B.T. Tsurutani, G.S. Lakhina, et al. A review of interplanetary discontinuities and their geomagnetic effects // *J. Atmos. Sol. Terr. Phys*. 2011, v. 73, p. 5–19. doi:10.1016/j.jastp.2010.04.001

3. E. Echer, B. Tsurutani, W. Gonzalez. Interplanetary origins of moderate (-100 nT $<$ Dst $\leq$ -50 nT) geomagnetic storms during solar cycle 23 (1996–2008) // *J. Geophys. Res. Space Physics*. 2013, v.118, p. 385–392. doi: 10.1029/2012JA018086

4. E. Kilpua, K. Lumme, A. Andreeova, et al. Properties and drivers of fast interplanetary shocks near the orbit of the Earth (1995–2013) // *J. Geophys. Res. Space Physics.* 2015, v. 120, p. 41120-4125. doi:10.1002/2015JA021138

5. L. Jian, C.T. Russell, J.G. Luhmann, et al. Properties of Stream Interactions at One AU During 1995–2004 // *Sol. Phys*. 2006, v. 239 p. 337–392. https://doi.org/10.1007/s11207-006-0132-3

6. I.G Richardson. Solar wind stream interaction regions throughout the heliosphere // *Sol. Phys*. 2018, v. 15, id. 1. https://doi.org/10.1007/s41116-017-0011-z

7. Z. Zhong, C. Shen, Y. Chi, et al. Prediction for Arrival Time and Parameters of Corotation Interaction Regions using Earth–Mars Correlated Events from Tianwen-1, MAVEN, and Wind Observations // *ApJ*. 2024, v. 965, id. 114. DOI 10.3847/1538-4357/ad2fab

8. J.T. Gosling, V.J. Pizzo. Formation and Evolution of Corotating Interaction Regions and their Three Dimensional Structure // *Space Sci. Rev*. 1999, v. 89(1/2), p. 21-52. https://doi.org /10.1023/A:1005291711900

9. A.P. Rouillard, M. Lockwood. The Latitudinal Effect of Corotating Interaction Regions on Galactic Cosmic Rays // *Sol. Phys*. 2007, v. 245, p. 191–206. https://doi.org/10.1007/s11207-007-9019-1

10. B. Heber, T.R. Sanderson, M. Zhang. Corotating interaction regions // *Adv. Space Res.* 1999, v. 23, N 3, p. 567-579. https://doi.org/10.1016/S0273-1177(99)80013-1

11. M. Pick, N. Vilmer. Sixty-five years of solar radioastronomy: flares, coronal mass ejections and Sun–Earth connection // *Astron. Astrophys. Rev*. 2008, v. 16, p. 1-153. https://doi.org/10.1007/s00159-008-0013-x

12. Y. Chi, C. Shen, B. Luo, et al. Geoeffectiveness of stream interaction regions from 1995 to 2016 // *Space Weather.* 2018, v. 16, p. 1960-1971. https://doi.org/10.1029/2018SW001894

13. B. Yu, C.S. Scott, X. Xue, et al. A Signature of 27 day Solar Rotation in the Concentration of Metallic Ions within the Terrestrial Ionosphere // *ApJ*. 2021, v. 916, id. 106. DOI 10.3847/1538-4357/ac0886

14. C.J. Owen, R. Bruno, S. Livi, et al. The Solar Orbiter Solar Wind Analyser (SWA) suite // *A&A*. 2020, v. 642, id. A16. https://doi.org/10.1051/0004-6361/201937259

15. T.S. Horbury, H. O’Brien, I.C. Blazquez, et al. The Solar Orbiter magnetometer // *A&A*. 2020, v. 642, id. A9. https://doi.org/10.1051/0004-6361/201937257

16. M. Maksimovic, S.D. Bale, T. Chust, et al. The Solar Orbiter Radio and Plasma Waves (RPW) instrument // *A&A*. 2020, v. 642, id. A12. https://doi.org/10.1051/0004-6361/201936214

17. O. Kruparova, et al. Automated interplanetary shock detection and its application on WIND observations // *J. of Geophys. Res*. 2013, v. 118, issue 8, p. 4793. https://doi.org/10.1002/jgra.50468

18. M. Maksimovic, V. Krupar, O. Alexandrova. RPW-SCI-NTT-000243-LES – RPW Instrument: Definition of the In-Flight Burst Modes Detection Algorithms. 2015. https://rpw.lesia.obspm.fr/

19. J.W. Belcher, L.Jr. Davis. Large-amplitude Alfvén waves in the interplanetary medium, 2 // *J. Geophys. Res.* 1971, v. 76, id. 3534. https://doi.org/10.1029/JA076i016p03534

20. L.K. Jian, J.G. Luhmann, C.T. Russell, et al. Solar Terrestrial Relations Observatory (STEREO) Observations of Stream Interaction Regions in 2007 – C.T. Russell, et al. SoHeliospheric Current Sheets, Solar Cycle Variations, and Dual Observations // *Sol. Phys*. 2019, v. 294, id. 31. https://doi.org/10.1007/s11207-019-1416-8

21. D. Müller, O.C. Cyr, I. Zouganelis, et al. The Solar Orbiter mission: Science overview // *A&A*. 2020, v. 642, id. A1. https://doi.org/10.1051/0004-6361/202038467

22. C.C. Marirrodriga, A. Pacros, S. Strandmoe, et al. Solar Orbiter: Mission and spacecraft design // *A&A*. 2021, v. 646, id. A121. https://doi.org/10.1051/0004-6361/202038519

23. J.L. Bougeret et al. S/WAVES: The radio and plasma wave investigation on the STEREO mission // *Space Sci. Rev*. 2008, v. 136, p. 487-528. https://doi.org/10.1007/s11214-007-9298-8

24. J.L. Bougeret et al. WAVES: The radio and plasma wave investigation on the wind spacecraft // *Space Sci Rev*. 1995, v. 71, p. 231-263. https://doi.org/10.1007/BF00751331

25. R.C. Allen et al. Suprathermal particles from corotating interaction regions during the first perihelion pass of Solar Orbiter // *A&A*. 2021, v. 656, id. L2. https://doi.org/10.1051/0004-6361/202039870

Article received 14.04.2025

SBM1-РЕЖИМ ПРИЛАДУ RPW/SOLAR ORBITER ЯК ПОШУКАЧ НЕОДНОРІДНОСТЕЙ СОНЯЧНОГО ВІТРУ В МІЖПЛАНЕТНОМУ ПРОСТОРІ

Д.Л. Чечоткін, О.В. Дудник, О.В. Яковлєв

Розриви та неоднорідності у великомасштабних структурах сонячного вітру (СВ) є одними з основних джерел збурень, які передаються від Сонця до земної магнітосфери та є причиною різних явищ космічної погоди. Аналізується можливість використання тригерних подій SBM1-приладу RPW космічної місії Solar Orbiter як маркерів наявності областей стиснення та інших неоднорідностей потоків СВ. На прикладах показано, що неодноразові спрацьовування тригера SBM1 на інтервалі до чотирьох годин відбивають тонку структуру великомасштабних коливань параметрів СВ, і такі тригерні події можна використовувати як маркер знаходження космічного апарата в області стиснення.